BJRS

BRAZILIAN JOURNAL
OF
RADIATION SCIENCES
10-03 (2022) 01-18

Relative dose-response from solid-state and gel dosimeters through Monte Carlo simulations

Souza Neto[a] N., Quevedo[b] A., Alva-Sánchez[c] M.S., Pianoschi[b] T.

[a] *Medical Physics course, Federal University of Health Sciences of Porto Alegre, UFCSPA, 90050-170, Porto Alegre, RS, Brazil*

[b] *Department Health Science, Oeste Paulista University, UNOESTE, 17213-700, Jaú, SP, Brazil*

[c] *Department of Exact Science and Applied Social, Federal University of Health Sciences of Porto Alegre, UFSCPA, 90050-170 Porto Alegre, RS, Brazil*

mirko@ufcspa.edu.br

ABSTRACT

The present work compares the relative absorbed dose of some dosimetric materials for energies of 250 kV and 6 MV, using PENELOPE and MNCPX codes. The composition of GD-301, TLD-100, MAGIC, and MAGAT was simulated and disposed of in a phantom filled with water following reference conditions recommended by the TRS-398 protocol. Percentage depth dose (PDD) was used as a parameter of comparison. For both energy studies, the maximum difference of 2 % was found when comparing the values of PDDs in water obtained from experimental and simulation data before 6cm. After this depth, a maximum difference of up to 2.2% for 6 MV and 5.5 % for 250 kV was found. Ratios between simulated PDD and experimental PDD values showed a maximum difference in the build-up region, for 6 MV, due to high sensitivity from the incident fluency in the simulated and experimental conditions. The PDD ratios for 250 kV showed significant differences for solid-state than gel dosimeters. As the literature corroborates, there is depth angular dependence from the solid-state dosimeter for low energy. Even the differences showed for both codes, especially for lower energy, due to the cross-section database that implied the interaction probability for each Monte Carlo code. This method has been widely used to model radiation transport in several applications in medical physics, especially in dosimetry.

Keywords: **Glass dosimeter, luminescence dosimeters, Gel dosimeters, Monte Carlo codes.**

ISSN: 2319-0612
DOI: https://doi.org/10.15392/bjrs.v10i3.2046
Submitted: 2022-04-11
Accepted: 2022-09-05

1. INTRODUCTION

The present work analyzes two solid states (GD-301, TLD-100) and two gel dosimeters (MAGIC and MAGAT) to evaluate some features between them.

Some glasses irradiated by ionization radiation are excited and can emit visible light when stimulated by ultraviolet radiation. This phenomenon is called radiophotoluminescence (RPL). A significant characteristic of this dosimeter is that luminescence centers in this material do not disappear after being read. Radiophotoluminescence has been studied since the 1950s [1-5]. In the following decade, improved glass formulations showed increased sensitivity avoiding noise efficiency [6,7], allowing advanced glass formulations and sophisticated optoelectronics [8]. The chemical composition of the GD-301 is described in table 1; since the compost silver-activated phosphate glass is exposed to ionizing radiation, RPL centers appear and after submitting to a pulsed ultraviolet laser beam, it emits orange luminescence, which is proportional to the absorbed dose [9]. The reading of glass dosimeters is quite complex and requires the separation of rapid photoluminescence from the glass, mainly emitted within 1 μs of the excitation pulses, actual radiophotoluminescence signal collected up to 40 μs of pulses, and longer decay signal due to contamination effects on the surface.

A wide range of thermoluminescence (TL) materials is available commercially; the most popular being TLD-100 due to its capacity for measurements when exposed at low and higher energies [10,11]. When a TL material is excited by radiation, there is a possibility of trapping and storing energy. If this material is heated up, the trapped energy can be realized in the form of photons (visible light), which is proportional to the absorbed dose. The simplest method of analysis involves the integration of the emission curve, that is, the signal strength as a function of the temperature of the sample in a predetermined temperature range [12]. The most complex method involves computerized deconvolution of the emission curve, separating its emission peaks coupled components with analytical fund estimates from the curve. It is the knowledge that the process of reading the TL dosimeters is destructive, in contrast with the RPL dosimeters. The argument is that once a detector is heated to a maximum reading temperature, the electron traps are emptied, and the dose information is cleared. Also, the material TL can be irradiated with light source ultraviolet to retrieve information about the dose from these deep traps. Since there are traps at high-temperature depths that are filled with electrons during irradiation but are not emptied during reading [13].

Different formulations of gel dosimetry have been proposed for applications in medical physics with several beams and quality differences [14,15]. Generally, these dosimeters consist of monomers dissolved in an aqueous gel matrix with approximately 90% water composition, corroborating its equivalence in water [16–19]. When a polymeric gel sample is subjected to ionizing radiation, the polymerization can be quantified by various image methods such as magnetic resonance images (MRI), X-ray computer tomography, optical CT, ultrasound, and vibrational spectroscopy. MRI has been the most common method used to date [20].

The significant development of polymeric dosimetry occurred when MAGIC (Methacrylic and Ascorbic acid in Gelatin Initiated by Copper) was proposed [21] and other formulations have been proposed [22–24]. Polymeric gels are prepared by mixing the monomers at a specific temperature; after that, the mix is transferred to phantoms, glass tubes, or another container sealing and kept in the refrigerator approximately 24 h after irradiation [25,26]. New investigations of polymeric formulations were proposed, such as the MAGAT (Methacrylic Acid Gelatin And Tetrakis (hydroxymethyl) phosphonium chloride), also composed of a gel matrix made of water and gelatin and some monomers. Some investigations have reported its characteristics as tissue-equivalent highest dosimeter sensitivity [20,21,27–29], improving better than MAGIC polymer gels [22,30].

To guarantee the dosimetric characteristics of new dosimeter materials is necessary to perform experiment tests; however, these procedures require excessive time and high cost. Thus, computational simulations can be performed as an alternative to experimental methods to obtain valuable information with the prediction of computational results [31-35]. Several Monte Carlo-based codes are used in physics research [36–41]. The MCNPX code was developed to study particle physics and nuclear reactions, so they simulate an extensive set of particles in a broad energy spectrum [42–45] and many medical physics applications [46–50]. On the other hand, codes such as PENELOPE focus on the transport of charged particles and photons to medical applications and simulation of accelerator linear in the context of radiation protection and dosimetry [51–55]. Thus, the present work uses simulation codes to evaluate the dose-response of the solid-state and gel dosimeters in low and high energy through two Monte Carlo codes.

2. MATERIALS AND METHODS

The present work used two Monte Carlo codes, PENELOPE, version 2008 [56], and MCNPX, version 2.7.0 [57], for all simulation conditions. Both codes contain in their database some materials and allow the construction of complex materials through their chemical compositions. Both codes contain water material used in the present work following the recommendations of the TRS 398 protocol [58].

2.1. Dosimetric materials

To simulate the dosimetric materials of GF-301, TLD-100, MAGIC, and MAGAT were using its physics/chemical characteristic like weight fractions and density, as shown in Table 1. These characteristics are input data into a code to simulate a certain dosimeter.

Table 1: Chemical Composition of Dosimeters.

Dosimeters	**Chemical Composition (weight fractions)**						**Density (g/cm³)**
GD-301 (6,59)	P	O	Al	Na	Ag		2.610
	$3.155x10^{-1}$	$5.116x10^{-1}$	$6.120x10^{-2}$	$1.100x10^{-1}$	$1.700x10^{-3}$		
TLD-100 (6)	Li	F	Mg	Ti			2.635
	$2.670x10^{-1}$	$7.320x10^{-1}$	$9.5238x10^{-4}$	$4.6719x10^{-5}$			
MAGIC (60)	H	C	N	O	S	Cu	1.037
	$1.047x10^{-1}$	$8.570\ x10^{-2}$	$1.150x10^{-2}$	$7.984x10^{-1}$	$2.568x10^{-6}$	$5.090x10^{-6}$	
MAGAT (60)	H	C	N	O	P	Cl	1.032
	$1.042x10^{-1}$	$8.540x10^{-2}$	$1.150x10^{-2}$	$7.928x10^{-1}$	$1.500x10^{-3}$	$1.700x10^{-3}$	

2.2. Beam spectrum

Two-photon beams, used in the service of radiotherapy, were chosen: 250 kV [61] representing the spectrum for orthovoltage devices, with effective energy of 140 keV, dedicated to the treatment of superficial tumors and 6 MV photon beams [62] with effective energy of 1.71 MeV, representing typical energy applied for different treatments in a Brazilian radiotherapy clinic. As shown in figure 1, the relative fluence from each spectrum is input in both simulations of Monte Carlo codes.

Figure 1: *Spectrum beam for 250 kV and 6 MV photons*

(a) (b)

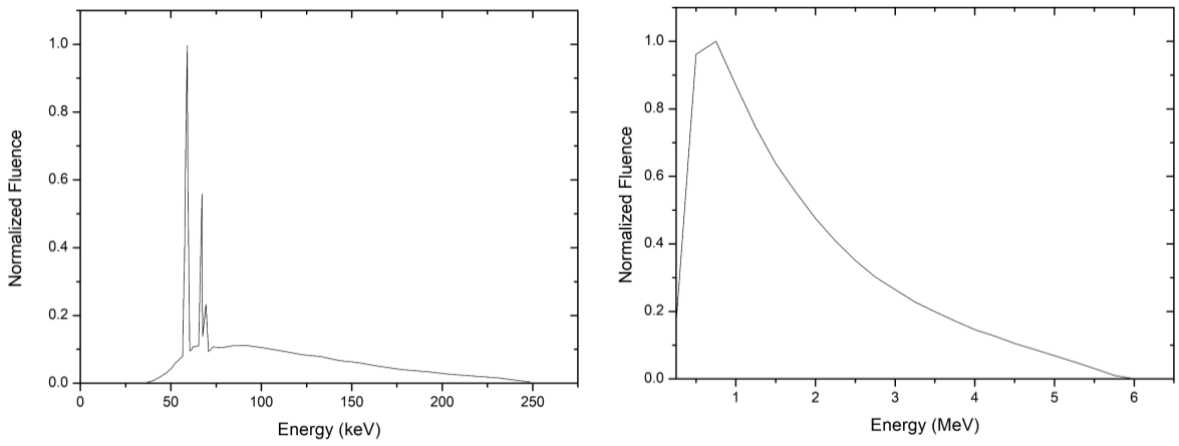

2.3. Simulation conditions

For all simulations, a phantom of 20 x 20 x 21cm³ with water material was used for both simulation codes, respectively. The simulation conditions a field size of 10 x 10 cm^2, a source-surface distance of 100 cm for 6 MV, and 40 cm for 250 kV, following the recommendations of the TRS 398 protocol [58].

Cylindrical detectors with a sensitive volume of 8.65 mm^3 were created with the respective simulation code with the materials TLD-100 and GD-301. Each detector was positioned at an interval from 0.5 cm until 20 cm in the phantom filled with water. Thus, each detector was simulated in a determinate depth, energy and simulation code.

The whole phantom and the sensitive volumes were filled with the same material to simulate the MAGIC and MAGAT gels. In the simulations carried out in the MCNPX, *F8 tallies were used. This type of tally stores the energy deposition information used to calculate the absorbed dose in a sensitive volume. From PENELOPE returned the energy deposition value in all bodies described in the geometry file "penmain-res". 2.5 x 10^7 particles were simulated for the materials: water, GD-301, and TLD-100, and 1.5 x 10^7 particles for MAGIC and MAGAT. The simulations were validated through PDD curves in water, first performed for each code and compared with theoretical data.

2.4. Data analysis

PDD curves were determined from the simulation results to compare the dose-response of the detectors used in the present work. The quantity PDD [18,52,63] can be obtained with the ratio

between the absorbed dose at any detector position at depth related to the absorbed dose value at the maximum ionization depth along the central field axis.

The experimental PDD curves for 250 kV and 6 MV photon beams obtained from the experimental data were used to validate the simulated condition used in this work. The PDDs value for 250 kV was provided by Hospital de Amor, Barretos, São Paulo-Brazil and for PDDs for 6 MV was provided by the radiotherapy department of Hospital Santa Rita do complexo da Santa Casa de Misericórdia de Porto Alegre, Rio Grande do Sul - Brazil. In addition, PDD ratios between simulated (for each dosimeter) and experimental PDD (in water) were compared. These data were obtained in the commissioning of the x-ray apparatus following the TRS-398 protocol.

3. RESULTS AND DISCUSSION

The output values corresponding to each simulation were performance PDD curves using the water material, which were compared with experimental data. Comparing these curves can help validate the conditions used in this work. Figures 2 and 3 show the PDD curves for energies of 6 MV and 250 kV photon beams.

Figures 2 and 3 show that both simulation codes reproduce the experimental data with a difference of less than 2% for 6 MV; this difference is comparable to Marioti et al. [18] and Suda et al. [70]. For 250 kV photon beam, the difference from 3.3% to 5.5% for PENELOPE code and 2.2% to 3.2% for MCNPX were found at depths between 6 and 11 cm, relative to experimental data. This difference is assumed due to the range of the electrons that make the dose deposition smaller for lower energy. Resulting in a drastic reduction of particle counting in the detectors farthest from the surface, which affects both codes, still due to dependencies on energy, depth, and angulation from the dosimeters and the cross-section data implementation by each simulation code [65]. It is worth mentioning that the difference between the simulation and experimental values of PDD shows differences of less than 2 %, up to 6 cm.

Figure 2: *PDD curve for 10x10 cm² of field size, in terms of water and for 6 MV photons beam.*

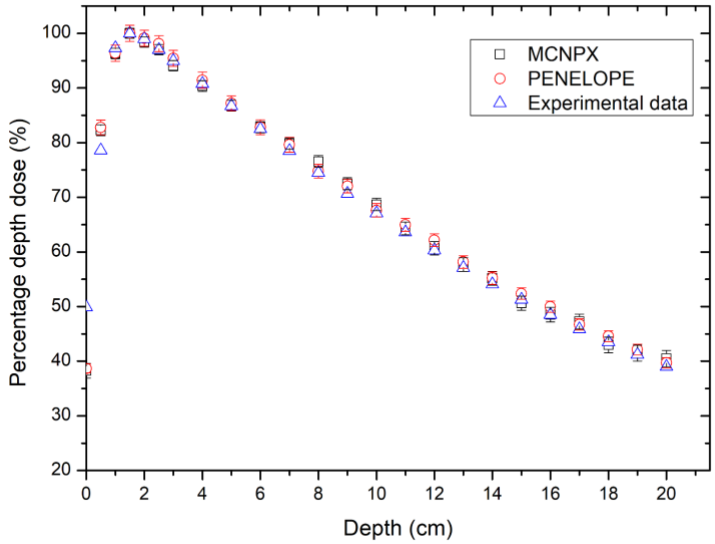

Figure 3: *PDD curve for 10x10 cm² of field size, in terms of water and for 250 kV photons beam.*

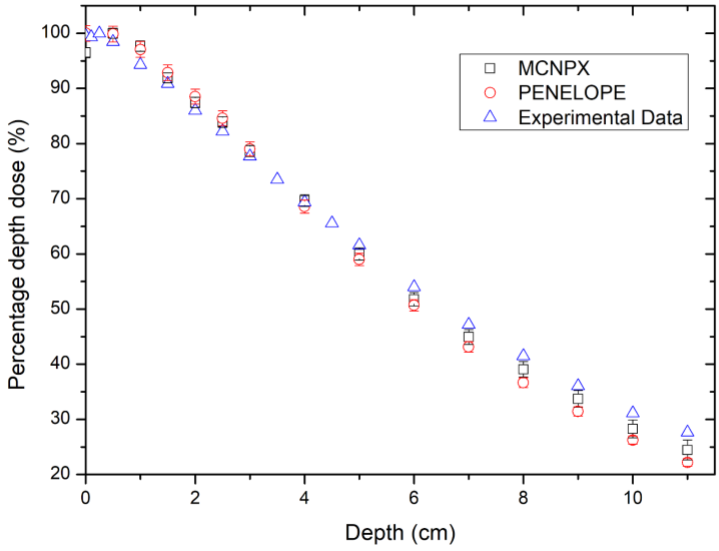

Figures 4 and 5 show the PDD curves obtained with the two codes used and for TLD, GD-301, MAGAT, and MAGIC materials simulated, to 6 MV (Figure 4) and 250 kV (Figure 5), respectively·

Figure 4: *PDD curves simulated in reference conditions for 6 MV photons with (a) TLD, GD-301, and (b) MAGAT and MAGIC simulated material.*

(a) (b)

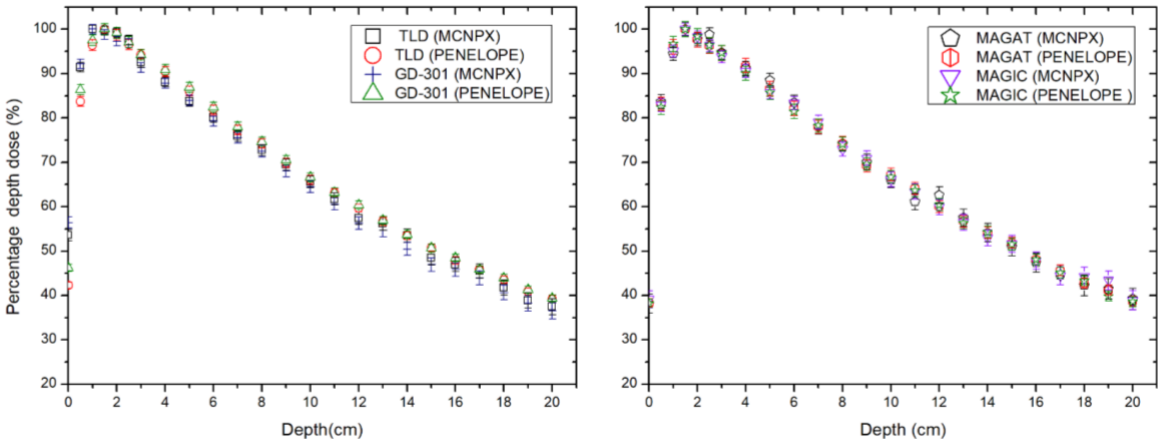

Figure 5: *PDD curves simulated in reference conditions for 250 kV photons with (a) TLD, GD-301, and (b) MAGAT and MAGIC simulated material*

(a) (b)

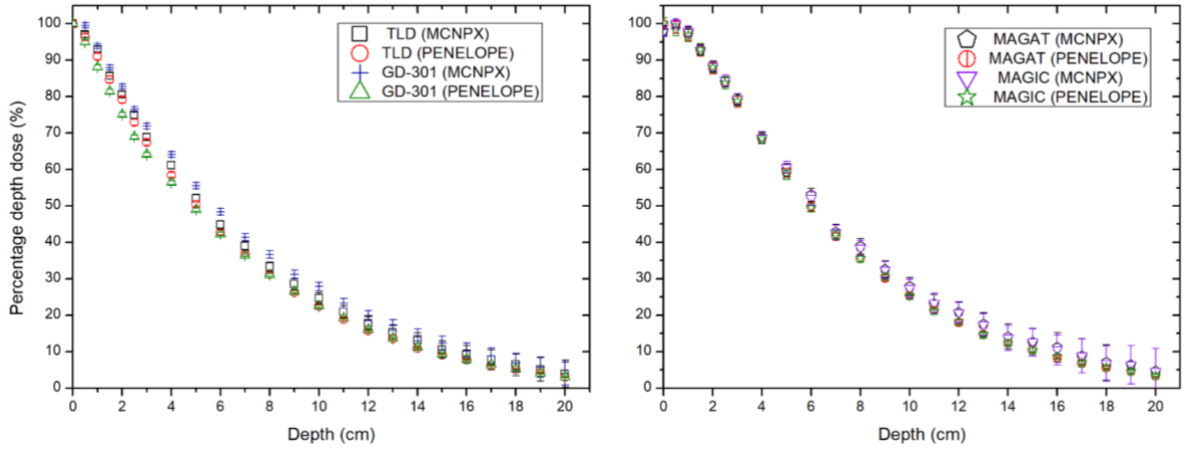

The behavior of PDD curves shown in figures 4 and 5 tend to an expected dose deposition in-depth for each energy beam used. The results were grouped into solid-state and gel dosimeters to evaluate the dose-response of each simulation code and relative equivalence in water.

A maximum percentage difference of up to 10% was found when comparing PDD values for the solid-state dosimeter before the build-up region and of 3.5% in deeper regions along the depth dose deposition for 6 MV photon beam, as shown in figure 4a. For the 250 kV photon beam, a maximum

percentage difference was 7.5%, approximately in a 2.5 cm depth from the GD-301 PDD curves, as shown in figure 5a. Despite the difference, the results obtained in this work are according to the literature[6].

In the second group, gel dosimeter materials, when comparing the PDDs curves obtained with the two codes simulation, a maximum percentage difference of up to 2.5% was found from the PDD obtained with the MAGAT material for 6 MV. For a 250 kV photon beam, a maximum percentage difference was 3.2%, approximately, in an 8 cm depth from the MAGAT PDD curves, as shown in figure 5b.

Despite the MCNPX and PENELOPE codes having been useful to simulate photon–electron transport through matter for kV and MV energy range applications in medical physics, the results showed significant differences, especially for the beam of 250 kV. A possible reason is the differences in cross-section values from the simulation codes, especially for lower photon energies and high atomic number materials [64,65], as shown in figure 5, since the GD-301 and TLD-100 have 12 and 8.3 effective atomic numbers, respectively [66].

By comparing the PDD determined versus the experimental data, figures 6 and 7 were generated as the ratio between PDD values obtained by simulation (PDDsim.) and PDD got experimentally in terms of water (PDDexp.) in the function of the depth of phantom.

Figure 6: *PDD ratios between simulated and experimental values in reference conditions for 6 MV photons simulated with (a) MCNPX and (B) PENELOPE.*

(a) (b)

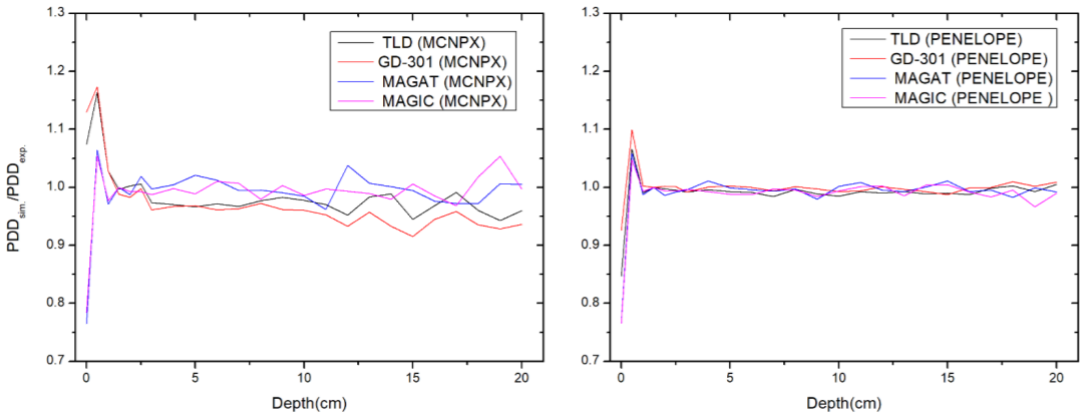

Figure 7: *PDD ratios between simulated and experimental values in reference conditions for 250 kV photons simulated with (a) MCNPX and (B) PENELOPE.*

(a) (b)

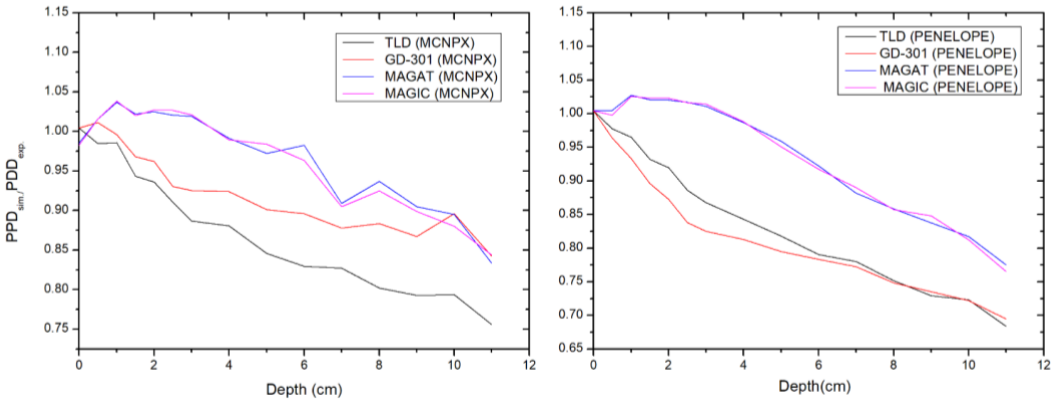

The significant discrepancies are shown in Figures 6a and 6b relative to experimental data, which are in a few centimeters of depth, possibly due to the entrance dose being susceptible to differences between the incident fluency in the simulated and experimental conditions [18,70]. According to literature data, the material dosimeter used TLD-100 and GD-301 did not show energy dependence for 6 MV photon beam [10,67]. A similar response is observed for MAGIC and MAGAT dosimeter materials.

The PDD ratios shown in figure 7, for 250 kV, reflect significant differences for state-solid rather than gel dosimeters; even state-solid detectors (TLD-100 and GD-301) are used in some applications in medical physics [10,11,68]. Nevertheless, dosimetric gels are widely used in medical physics research (16–18,69), with differences increasing in depth, as shown in figures 5 and 7.

Oscillations between the ratio of the PDDs were observed with more evidence for MCNPX simulation than for the PENELOPE, as shown in figure 6, which can be explained due to the code sensibility, particle numbers used and the shape of the dosimeter dimensions. Still, the absolute discrepancy between the data is similar to the PENELOPE. Especially for low energy, the differences are more considerable due to the implementation of the electron transport algorithms that each code simulation applied. Since any change, even minimally, in the spectrum causing the low-energy to scatter component to become more pronounced in depth [71], still associated with materials such as high atomic numbers that showed photon energy dependence of the quotient of the mass-energy absorption coefficients [72]. The spectral analysis based on the total and secondary spectra of photons

at depth by simulation can help make the correction that can be applied relatively simply, thus softening the differences in depth. As depth increases, the total spectra show a more significant number of particles with lower energies, which shifts the average energy of the simulated beam reaching that depth to a lower value than the average energy of the incident beam [73].

4. CONCLUSION

The MCNPX and PENELPOLE, Monte Carlo codes used in this work simulated the radiation transport into dosimetric materials to a specific low and high-energy x-ray beam. The dose-response of the dosimetric materials simulated, GF-301, TLD-100, MAGIC, and MAGAT, were analyzed through the PDD curves and showed similar behavior in simulation conditions for applications in radiotherapy. The ratio between PDDsim. /PDDexp., showed more differences in the few centimeters from the entrance of the simulated phantom for 6 MV photon beam and for both codes, which corroborates with the literature, especially for gel dosimeters. For 250 kV photon beam differences significant were found, especially for the solid-state dosimetric materials. When dealing specifically with lower energies were found significant differences simulating the GD-301 and TLD-100 materials. Since these divergences between codes are expected to use different nuclear data and cross-sections. These data demonstrate that the simulation environments developed for this research faithfully reproduce the actual irradiation conditions with x-ray beams and, therefore, be used in future work to study new dosimetric materials and research in radiotherapy.

ACKNOWLEDGMENT

Special thanks to Ph.D. Professor Maurício Tizziani Pazianotto who collaborated with this research assisting with the use of the MCNPX and the workgroup appreciated the contributions from Hospital de Amor, Barretos, São Paulo-Brazil, the radiotherapy department of Hospital *Santa Rita do complexo da Santa Casa de Misericórdia de Porto Alegre, Rio Grande do Sul - Brazil* and The Laboratory of Medical Physics of the Federal University of Health Sciences of Porto Alegre.

REFERENCES

[1] CHAND, S.; MEHRA, R.; CHOPRA, V. Recent developments in phosphate materials for their thermoluminescence dosimeter (TLD) applications. Luminescence, v. 36(8), p. 1808–1817, 2021.

[2] GUERIN, G.; CHRISTOPHE, C.; PHILIPPE, A., MURRAY, A.S.; THOMSEN, K. J.; TRIBOLO, C.; ET AL. Absorbed dose, equivalent dose, measured dose rates, and implications for OSL age estimates: Introducing the Average Dose Model. Quat Geochronol, v. 41, p. 163–173, 2017.

[3] NEZHAD, Z.A. A review study on the application of gel dosimeters in low energy radiation dosimetry. Appl Radiat Isot, v. 179, p. 110015, 2019.

[4] PODGORSAK, E.B. Radiation Physics for Medical Physicists. 3rd ed. Springer, 2016.

[5] OLIVEIRA, L. C.; MILLIKEN, E. D.; YUKIHARA, E. G. Development and characterization of MgO: Nd,Li synthesized by solution combustion synthesis for 2D optically stimulated luminescence dosimetry. J Lumin, v. 133, p. 211–216, 2013.

[6] BENALI, A-H.; MEDKOUR, ISHAK-BOUSHAK, G.; NOURREDDINE, A.; ALLAB, M. Comparison of RPL GD-301 and TLD-100 detectors responses by Monte Carlo simulation. EPJ Web of Conferences, v. 100, p. 02001, 2015.

[7] PIESCHI, E.; BURGKHARDT, B.; FISCHER, M.; RÖBER, H. G.; UGI, S. Properties of Radiophotoluminescent Glass Dosemeter Systems Using Pulsed Laser UV Excitation. Radiation Protection Dosimetry, v.17, p. 293–297, 1986.

[8] YAMAMOTO, T. RPL Dosimetry: Principles and Applications. AIP Conference Proceedings, 2011. p. 217–230.

[9] RAH, J-E.;OH, D.H.; SHIN, D.; KIM, D-H.; J. I.; YH, K. I. M.; JW, ET AL. Dosimetric evaluation of a glass dosimeter for proton beam measurements. Appl Radiat Isot, v. 70, p. 1616–1623, 2012.

[10] WESOLOWSKA, P. E.; COLE, A.; SANTOS, T.; BOKULIC, T.; KAZANTSEV, P.; IZEWSKA, J. Characterization of three solid states dosimetry systems for use in high energy photon dosimetry audits in radiotherapy. Radiat Meas, v. 106. p. 556–562, 2017.

[11] GHONEAM, S. M.; MAHMOUD, K. R.; DIAB, H. M.; EL-SERSY, A. Studying the dose level for different X-ray energy conventional radiography by TLD-100. Appl Radiat Isot, v. 181, p. 110066, 2022.

[12] HOROWITZ, Y. S.; MOSCOVITCH, M. Highlights and pitfalls of 20 years of application of computerized glow curve analysis to thermoluminescence research and dosimetry. Radiat Prot Dosim, v. 153, p. 1–22, 2013.

[13] MOSCOVITCH, M.; BENEVIDES, L.; ROMANYUKHA, A.; HULL, F.; DUFFY, M.; VOSS, S, ET AL. The applicability of the PTTL dose re-analysis method to the Harshaw LiF:Mg,Cu,P material. Radiat Prot Dosim, v. 144, p. 161–164. 2011.

[14] BALDOCK, C.; DE DEENE, Y.; DORAN, S.; IBBOTT, G.; JIRASEK, A.; LEPAGE, M, ET AL. Polymer gel dosimetry. Phys Med Biol, v. 55, p, R1–63, 2010.

[15] FARHOOD, B.; GERAILY, G.; ABTAHI, S. M. M. A systematic review of clinical applications of polymer gel dosimeters in radiotherapy. Appl Radiat Isot, v. 143, p. 47–59, 2019.

[16] ALVA, M.; MARQUES, T.; SCHWARCKE, M.; RODRIGUES, L. N.; BAFFA, O.; NICOLUCCI, P. A Water-equivalent calibration of 192Ir HDR Brachytherapy source using MAGIC polymer gel. IFMBE Proceedings, v. 25, p. 248–251, 2009.

[17] ALVA, M.; PIANOSCHI, T.; MARQUES, T.; SANTANNA, M. M.; BAFFA, O.; NICOLUCCI, P. Monte Carlo Simulation of MAGIC- f gel for Radiotherapy using PENELOPE. J Phys Conf Ser, v. 250, p. 012067, 2010.

[18] MARIOTTI, V.; GAYOL, A.; PIANOSCHI, T.; MATTEA, F.; VEDELAGO, J.; PEREZ, ET AL. Radiotherapy dosimetry parameters intercomparison among eight gel dosimeters by Monte Carlo simulation. Radiat Meas, v. 190, p. 109782, 2022.

[19] QUEVEDO, A.; LUO, G.; GALHARDO, E.; PRICE, M.; NICOLUCCI, P.; GORE, JC, ET AL. Polymer gel dosimetry by Nuclear Overhauser Enhancement (NOE) magnetic resonance imaging. Phys Med Biol, v. 63, p. 5NT03, 2018.

[20] HURLEY, C.; VENNING, A.; BALDOCK, C. A study of a normoxic polymer gel dosimeter comprising methacrylic acid, gelatin and tetrakis (hydroxymethyl) phosphonium chloride (MAGAT). Appl Radiat Isot, v. 63, p. 443–456, 2005.

[21] FONG, P. M.; KEIL, D. C.; DOES, M. D.; GORE, J. C. Polymer gels for magnetic resonance imaging of radiation dose distributions at normal room atmosphere. Phys Med Biol, v. 46, p. 3105–3113, 2001.

[22] DE DEENE, Y.; HURLEY, C.; VENNING, A.; VERGOTE, K.; MATHER, M.; HEALY, B. J.; ET AL. A basic study of some normoxic polymer gel dosimeters. Phys Med Biol, v. 47, p. 3441–3463, 2002.

[23] GUSTAVSSON, H.; BÄCK, S. A. J.; MEDIN, J.; GRUSELL, E,; OLSSON, LE. Linear energy transfer dependence of a normoxic polymer gel dosimeter investigated using proton beam absorbed dose measurements. Phys Med Biol, 49, p. 3847–3855, 2004.

[24] FERNANDES, J. P.; PASTORELLO, B. F.; ARAUJO, D. B.; BAFFA, O. Formaldehyde increases MAGIC gel dosimeter melting point and sensitivity. Phys Med Biol, v. 53, p. N53–N58, 2008.

[25] OSMAN, H.; GÜMÜS, H. Stopping power and CSDA range calculations of electrons and positrons over the 20 eV–1 GeV energy range in some water equivalent polymer gel dosimeters. Appl Radiat Isot, v. 179, p. 110024, 2022.

[26] BRAHIMIMOUSSA, S.; BENAMAR, M. E. A.; LOUNISMOKRANI, Z. Characterization of the chemical and structural modifications induced by gamma rays on the MAGIC polymer gel. Rad Phys Chem, v. 166, p. 108451, 2020.

[27] MUSTAQIM, A. S.; YAHAYA, N.Z .; RAZAK, N. N. A.; ZIN, H. The dose enhancement of MAGAT gel dosimeter doped with zinc oxide at 6 MV photon beam. Rad Phys Chem, v. 172 p. 108739, 2020.

[28] RAZAK, N. N.; RAHMAN, A. A.; KANDAIYA, S.; MUSTAFA, I. S.; MAHNOUD, A. A.; YAHAYA, N. Z. Optimisation of the MAGAT gel dosimeter compositions. Int J Radiat Res, v. 14, p. 305–311, 2016.

[29] RESENDE, T. D.; LIZAR, J. C.; DOS SANTOS, F. M.; BORGES, L. F.; PAVONI, JF. Study of the formulation optimization and reusability of a MAGAT gel dosimeter. Physica Medica, v. 63, p. 05–11, 2019.

[30] NATANASABAPATHI, G.; WARMINGTON, L.; WATANABE, Y. Evaluation of two calibration methods for MRI-based polymer gel dosimetry. Appl Radiat Isot, v. 174, p. 109754, 2021.

[31] BALCAZA, V. G.; CAMP, A.; BADAL, A.; ANDERSSON, M.; ALMEN, A.; GINJAUME, M, ET AL. Fast Monte Carlo codes for occupational dosimetry in interventional radiology. Physica Medica, v. 85, p. 166–174, 2021.

[32] BAGHANI, H. R.; ROBATJAZI, M. Theoretical and Monte Carlo-based Kerma factor evaluation for various thermoluminescence (TL) dosimetry materials over a wide range of photon energies. Eur Phys J Plus, v. 136, 2021.

[33] ALVAREZ, D. S. A.; WATSON, P. G. F.; POPOVIC, M.; HENG, V. J.; EVANS, M. D. C; SEUNTJENS, J. Monte Carlo calculation of the TG-43 dosimetry parameters for the INTRABEAM source with spherical applicators. Phys Med Biol, v. 66, p. 215017, 2021.

[34] MASSERA, R. T.; THOMSON, R. M, TOMAL, A. Technical note: MC-GPU breast dosimetry validations with other Monte Carlo codes and phase space file implementation. Med Phys, v. 49, p. 244–253, 2022.

[35] ANDREO, P. Monte Carlo simulations in radiotherapy dosimetry. Radiat Oncol.;13, 121, 2018.

[36] SARRUT, D.; ETXEBESTE, A.; MUNOZ, E.; KRAN, N.; LETANG, J. M. Artificial Intelligence for Monte Carlo Simulation in Medical Physics. Front Phys, v. 9, p. 738112, 2021.

[37] KOIVUNORO, H.; SIISKONEN, T.; KOTILUOTO, P.; AUTERINEN, I, HIPPELAINEN, E.; SAVOLAINEN, S. Accuracy of the electron transport in MCNP5 and its suitability for ionization chamber response simulations: A comparison with the EGSNRC and PENELOPE codes. Med Phys, v. 39, p. 1335–1344, 2012.

[38] KHAN, H.; KORESHI, Z. U.; AZIZ, U.; SHEIKH, S. R.; AHMAD, S. A. Energy deposition and dose enhancement using Monte Carlo derivative sampling: applications in brachytherapy. J Natl Sci Found, v. 49, p. 493–501, 2021.

[39] YANI, S.; TURSINAH, R.; RHANI, M. F.; HARYANTO, F.; ARIF, I. Comparison between EGSnrc and MCNPX for X-ray target in 6 MV photon beam. Journal of Physics Conference Series, v. 1127, p. 012014, 2019.

[40] ARCHAMBAULT, J. P. Monte Carlo calculations of electrons impinging on a copper target: A comparison of EGSnrc, Geant4 and MCNP5. Appl Radiat Isot, v. 132, p. 129–134, 2018.

[41] PARTANEN, M.; OJALA, J.; NIEMELA, J.; BJORKQVIST, M.; KEYRILAINEN, J.; KAPANEN, M. Comparison of two Monte Carlo-based codes for small-field dose calculations in external beam radiotherapy. Acta Oncol, v. 56, p. 891–893, 2017.

[42] SEDLACKOVA, K.; SAGATOVA, A.; ZAT'KO, B.; NECAS, V.; SOLAR, M.; GRANJA, C. MCNPX simulations of the silicon carbide semiconductor detector response to fast neutrons from D-T nuclear reaction. In: Proceedings of the 2015 International Conference on Applications of Nuclear Techniques (CRETE15). Crete, Greece: Erickson, A; Hamm, M; Rahnema, F; Zhang, D, International Journal of Modern Physics-Conference Series; vol. 44, 2016.

[43] MAROUFKHANI, F.; ABTAHI, S. M. M.; KAKAVAND, T. Assessment of secondary particles in breast proton therapy by Monte Carlo simulation code using MCNPX. Int J Radiat Res, v. 19, p. 23–29, 2021.

[44] OLIVEIRA, J. R. B.; MORALLES, M.; FLECHAS, D.; CARBONE, D.; CAVALLARO, M.; TORRESI, D.; ET AL. First comparison of GEANT4 hadrontherapy physics model with experimental data for a NUMEN project reaction case. Eur Phys J, v. 56, p. 153, 2020.

[45] DE NAPOLI, M.; ROMANO, F.; D'URSO, D.; LICCIARDELLO, T.; AGODI, C.;CANDIANO, G.; ET AL. Nuclear reaction measurements on tissue-equivalent materials and GEANT4 Monte Carlo simulations for hadrontherapy. Phys Med Biol, v. 59, p. 7643–7652, 2014;

[46] DISCHER, M.; EAKINS, J.;, WODA, C.; TANNER, R. Translation of the absorbed dose in the mobile phone to organ doses of an ICRP voxel phantom using MCNPX simulation of an Ir-192 point source. Rad Meas, v. 146, p. 106603, 2021.

[47] DE SAINT-HUBERT, M.; TYMINSKA, K.; STOLARCZYK, L.; BRKIC, H. Fetus dose calculation during proton therapy of pregnant phantoms using MCNPX and MCNP6.2 codes. Rad Meas, v. 149, p. 106665, 2021.

[48] PARK, E. T.; KIM, J. H.; KIM, C. S.; KANG, S. S. Characteristic evaluation of photoneutron in radiotherapy room using MCNPX. J Instrum, v. 10, p. P08007, 2015.

[49] ARCE, P.; LAGARES, J. I.; AZCONA, J. D.; AGUILAR-REDONDO, P. B. A proposal for a Geant4 physics list for radiotherapy optimized in physics performance and CPU time. Nucl Instrum Methods Phys Res A: Accel Spectrom Detec Assoc Equip, v. 964, p. 163755, 2020.

[50] SYAHIR, M. K.; FAHMI, M. R.; HASHIKIN, N. A. A. Dosimetric comparison between different radiotherapy protocols for prostate cancer using Geant4 Monte Carlo simulation. J Phys Conf Ser, v. 1497, p. 012018, 2020.

[51] VERBEEK, N.; WULFF, J.; BAUMER, C.; SMYCZEK, S.; TIMMERMANN, B.; BRUALLA, L. Single pencil beam benchmark of a module for Monte Carlo simulation of proton transport in the PENELOPE code. Med Phys, v. p. 48, p. 456–476, 2021.

[52] ALVA-SANCHEZ, M. S.; PIANOSCHI, T. A. Study of the distribution of doses in tumors with hypoxia through the PENELOPE code. Radiat. Phys. Chem, v. 167, p. 108428, 2020.

[53] SHEERAZ, Z.; CHOW, J. C. L. Evaluation of dose enhancement with gold nanoparticles in kilovoltage radiotherapy using the new EGS geometry library in Monte Carlo simulation. AIMS Biophys, v. 8, p. 337–345, 2021.

[54] SALVAT, F.; QUESADA, J. M. Collisions of Nucleons with Atoms: Calculated Cross Sections and Monte Carlo Simulation. Front Phys, v. 9, p. 733949, 2021.

[55] MASSERA, R. T.; FERNANDEZ-VAREA, J. M.; TOMAL, A. Impact of photoelectric cross section data on systematic uncertainties for Monte Carlo breast dosimetry in mammography. Phys Med Biol, v. 66, p. 115015, 2021.

[56] SALVAT, F.; FERNANDEZ-VAREA, J.; SEMPAU, J. PENELOPE-2008: a code system for Monte Carlo simulation of electron and photon transport. Nuclear Energy Agency OECD/NEA. Issy-les-Moulineaux, France. http://www.nea.fr. 2008;

[57] PELOWITZ, D. B. MCNPXTM USER'S MANUAL Version 2.6.0. Los Alamos National Laboratory, 2008.

[58] IAEA- International Atomic Energy Agency. Absorbed Dose Determination in External Beam Radiotherapy. An International Code of Practice for Dosimetry Based on Standards of Absorbed Dose to Water. Technical Reports Series No. 398. Vienna, 2000.

[59] ARAKI, F.; OHNO, T. The response of a radiophotoluminescent glass dosimeter in megavoltage photon and electron beams. Med Phys, v. 41, p. 122102, 2014.

[60] VENNING, A. J.; NITSCHKE, K. N.; KEALL, P. J.; BALDOCK, C. Radiological properties of normoxic polymer gel dosimeters. Med Phys, v. 32, p. 1047–1053, 2005.

[61] ROSENSCHÖLD, P. M.; NILSSON, P.; KNÖÖS, T. Kilovoltage x-ray dosimetry--an experimental comparison between different dosimetry protocols. Phys Med Biol, v. 53, p. 4431–4442, 2008.

[62] SHEIKH-BAGHERI, D.; ROGERS, D. W. O. Monte Carlo calculation of nine megavoltage photon beam spectra using the BEAM code. Med Phys, v. 29, p. 391–402, 2002.

[63] COHEN, M. Central axis depth dose data for use in radiotherapy. Br J Radiol Suppl, v. 11, p. 8–17, 1972.

[64] CINTRA, F. B.; YORIYAZ, H. Electron absorbed dose comparison between MCNP5 and PENELOPE code Monte Carlo code for microdosimetry. In: 2009 International Nuclear Atlantic Conference - INAC Rio de Janeiro, RJ, Brazil; 2009.

[65] HILL, R.; HEALY, B.; HOLLOWAY, L.; KUNCIC, Z.; THWAITES, D.; BALDOCK, C. Advances in kilovoltage x-ray beam dosimetry. Phys Med Biol, v. 59, p. R183–R231, 2014.

[66] BENALI, A-H.; ISHAK-BOUSHAKI, G. M.; NOURREDDINE, A-M.; ALLAB, M.; PAPADIMITROULAS, P. A comparative evaluation of luminescence detectors: RPL-GD-301, TLD-100 and OSL-AL2O3:C, using Monte Carlo simulations. J Instrum, v. 12, p. P07017, 2017.

[67] KNEZEVIC, Z.; STOLARCZYK, L.; BESSIERES, I.; BORDY, J. M.; MILJANIC, S.; OLKO, P. Photon dosimetry methods outside the target volume in radiation therapy: Optically stimulated luminescence (OSL), thermoluminescence (TL) and radiophotoluminescence (RPL) dosimetry. Rad Meas, v. 57, p. 9–18, 2013.

[68] TONGKUM, S.; SUWANPRADIT, P.; VIDHYARKORN, S.; SIRIPONGSAKUN, S.; OONSIRI, S.; RAKVONGTHAI, Y.; ET AL. Determination of radiation dose and low-dose protocol for digital chest tomosynthesis using radiophotoluminescent (RPL) glass dosimeters. Phys Med, v. 73, p. 13–21, 2020.

[69] BALDOCK, C. Review of gel dosimetry: a personal reflection. J Phys Conf Ser, v. 777, p. 012029, 2017.

[70] SUDA, Y.; HARIU, M.; YAMAUCHI R, ET AL. Direct energy spectrum measurement of X-ray from a clinical linac. J Appl Clin Med Phys, v. 22, p. 255-264, 2021.

[71] CARBORO, S. B.; FOLLOWILL, D. S.; HOWELL, R. M.; KRY, S. F. Variations in photon energy spectra of a 6 MV beam and their impact on TLD response. Med Phys. v. 38, p. 2619-2628, 2011.

[72] NDIMOFOR, C.; DIETRICH, H.; KAY, W.; ANTJE, R.; BJÖRN, P. Low-energy photons in high-energy photon fields – Monte Carlo generated spectra and a new descriptive parameter, Zeitschrift für Medizinische Physik, v. 21, p. 183-197, 2011.

[73] MARQUES T.; ALVA-SÁNCHEZ, M.; NICOLUCCI, P. Redução de incertezas em radioterapia utilizando simulação Monte Carlo: análise espectral aplicada à correção de dose absorvida. Radiol Bras. v. 43, p. 119–123, 2010.